Article:
Garg, A, Li, J, Hou, J et al. (2 more authors) (2017) A New Computational Approach for Estimation of Wilting Point for Green Infrastructure. Measurement, 111. pp. 351-358. ISSN 0263-2241

https://doi.org/10.1016/j.measurement.2017.07.026

A New Computational Approach for Estimation of Wilting Point for Green Infrastructure

[1]Ankit Garg, [2]Jinhui Li, [3]Jinjun Hou, [4]Christian Berretta, [5]Akhil Garg

[1]Department of Civil and Environmental Engineering, Shantou University, Shantou 515063, China
[2]Department of Civil and Environmental Engineering, Harbin Institute of Technology (HIT), Shenzhen, China
[3]School of Mathematics and Computational Science, Hunan University of Science and Technology, Xiangtan, Hunan 411201, China
[4]Department of Civil Engineering, University of Leeds, UK
[5]Department of Mechatronics Engineering, Shantou University, Shantou 515063, China

Abstract

Wilting point is an important parameter indicating the inhibition of plant transpiration processes, which is essential for green infrastructures. Generalization of wilting point is very essential for analyzing the hydrological performance of green infrastructures (e.g. green roofs, biofiltration systems) and ecological infrastructures (wetlands). Wilting point of various species is known to be affected by the factors such as soil clay content, soil organic matter, slope of soil water characteristic curve at inflection point (i.e., s index) and fractal dimension. Therefore, its practical usefulness forms the strong basis in developing the model that quantify wilting point with respects to the deterministic factors. This study proposes the wilting point model development task based on optimization approach of Genetic programming (GP) with respect to the input variables (soil clay content, soil organic matter, s-index and fractal dimension) for various type of soils. The GP model developed is further investigated by sensitivity and parametric analysis to discover the relationships between wilting point and input variables and the dominant inputs. Based on newly developed model, it was found that wilting point increases with fractal dimension while behaves highly non-linear with respect to clay and organic content. The combined effect of the clay and organic content was found to greatly influence the wilting point. It implies that wilting point should not be generalized as usually done in literature.

Keywords: Wilting point; soil fractal dimension; s index; clay content; organic matter; evolutionary algorithms

1. Introduction

The wilting point (θ_{pwp}) is the soil moisture below which transpiration process tends to inhibit. It is usually estimated as the moisture content at a soil matric potential of -1500 kPa (Hillel, 1971). It is one of the important parameters for design and analysis of crop performance especially under drought conditions [1-3]. Understanding of θ_{pwp} is one of the essential input functions, which is often used in interpretation of behavior of crop water consumption [4-6]. Furthermore, the knowledge of θ_{pwp} are is fundamental in analyzing the hydrological performance of green infrastructures for stormwater management (e.g. green roofs, biofiltration units) and ecological infrastructure (wetlands). The soil-water characteristics influence the evapotranspiration (ET) in green infrastructures which regulates their hydrological performance by regenerating the retention capacity of the system [7, 8]. Actual ET rates fall exponentially in proportion to the substrate's plant accessible moisture content limited by θ_{pwp} [9]. θ_{pwp} not only depends on plant species but also on soil characteristics such as fractal dimension (D_s), soil S index (slope of soil water characteristic curve (SWCC) at inflection point), clay content (C) and organic content (OM) [10-11]. This is because any changes in these soil properties could alter the soil-water relations and hence behavior of plant at wilting point (soil moisture) [12-13].

Several researchers have studied wilting point and its estimation from other soil parameters [14-15] explored relationships of wilting point with the soil parameters. However, the approach used was traditional linear regression approach which relies on the statistical assumptions. This approach however, may not be able to take into account the interaction effects of parameters such as D_s, S index, C and OM on $\theta_{pwp,}$ in the model. Alternatively, the intelligent data-driven methods such as genetic programming (GP), artificial neural network, support vector regression have achieved tremendous popularity [16-19] in developing the models in uncertain process behavior. These methods takes in the data of the input-output form and produces a model that predicts the output reasonably well.

Among these methods, the GP algorithm produces the explicit models that represents a function between the output and inputs of the process [20, 21]. Therefore, it would be interesting to explore the competency of the GP algorithm in modelling wilting point (θ_{pwp}) of the soil. In this study, the GP approach is proposed to formulate the relationship between θ_{pwp}, and D_s, S index, C and OM. The data for all the five parameters is obtained (with D_s estimated) from the experiments. This data is then input into the framework of GP to produce the wilting point model. The statistical metrics indicating the performance of the model is evaluated. The relationships between (θ_{pwp}) and each of the input is revealed by the sensitivity and parametric analysis on the best GP model. The complete statistical analysis is then used to check if the understanding obtained from the numerical analysis is in line with experimental study.

2. Soil properties and wilting point for various soils

In this study, θ_{pwp}, D_s, S index, clay content (C) and organic content (OM) were collected or estimated from several comprehensive databases [21 - 25]. This includes a total of 161 data sets to be analyzed. D_s was estimated from the fractal model proposed in [26] as shown in Eq.(1).

$$\theta_i = \phi\left(\frac{\psi_{aev}}{\psi_i}\right)^{D_s-3} \tag{1}$$

Where, ϕ is the soil porosity, Ds is the fractal dimension, θ_i is the water content, ψ_{aev} is the air entry value (kPa), and ψ_i is the matric potential (kPa) at the i^{th} time step of the measurement. Using the Laplace equation (relation between matric potential and pore radius of soil; e.g. $\psi_i \propto 1/r_i$ and $\psi_{aev} \propto 1/r_{max}$), Eq. (1), with Ds as the surface fractal dimension, represents the scaling of pore sizes retaining water at a certain capillary pressure. The relationship is represents the fractal version of Brooks and Corey model [27] (refer to Eq. (2))

$$\frac{\theta}{\theta_s} = \left(\frac{\psi}{\psi_{aev}}\right)^{-\lambda} \qquad (2)$$

Using correlation (λ=3-Ds) of λ and D_s proposed by Tyler and Wheatcraft [28], the value of surface fractal dimension was calculated for various soils using equations 1 and 2 and other parameters (θ_{pwp}, ψ_{aev} and λ) various databases selected in this study. Table 1 summarizes the statistics of both input parameters (D_s, S index, clay content and organic content) as well as output parameter to be modeled (θ_{pwp}).

Total of 60 data samples were obtained from this study. The four inputs/factors considered are fractal dimension (D_s) (x_1, %), S-index (x_2, unitless), clay content (x_3, min), organic content (x_4) and the output considered is wilting point (θ_{pwp}). Fig. 1 shows the nature of measurements of wilting point of soil. Higher variations of the data from Fig. 1 show that the wilting point data is inhibited with non-linearity because it is influenced by the several input factors. Fig. 2 shows the distribution (mean, median, maximum and minimum) of the four inputs and the wilting point. This accounts for higher non-linearity and interaction effect in the data. Choosing the appropriate training data set is important for faster and good learning capability of the GP approach. Therefore, based on the understanding of preliminary studies [20], the authors have applied 20-fold cross-validation algorithm for the generation of random 20 training and corresponding 20 test data sets [20]. This algorithm is well known for dividing the data set into training (75%, 40 samples) and testing in such a way that the samples considered for training are inside domain of the test data set. The formulated wilting point model is then tested on the remaining 20 testing samples to determine the robustness in its prediction values.

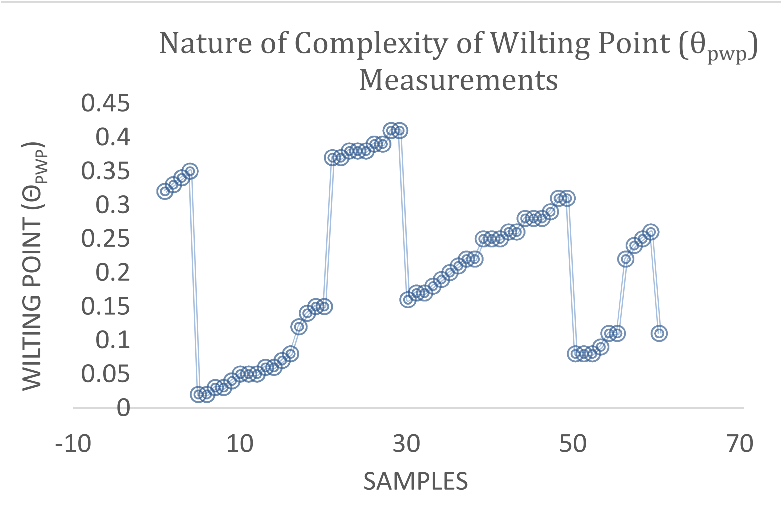

Fig. 1 Line plot showing the nature of wilting point measurements

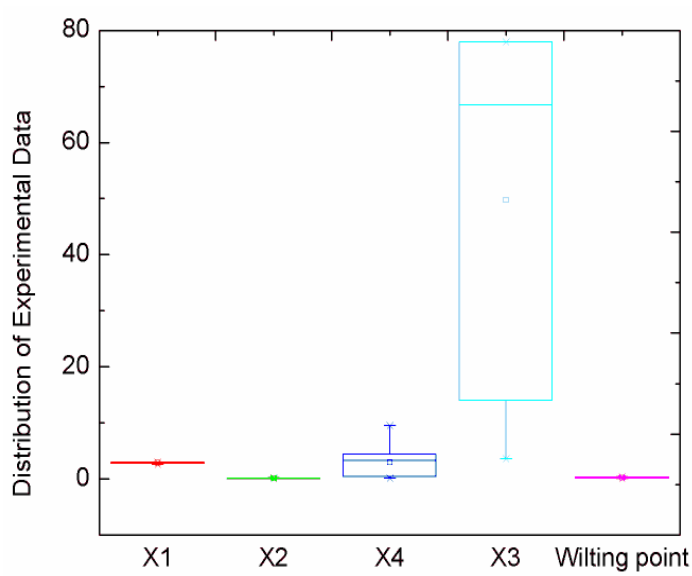

Fig. 2 Distribution of experimental comprising of inputs and wilting point

3. Design of Genetic programming based wilting point model (GP_W)

This manuscript introduces evolutionary framework of Genetic programming (GP) (Fig. 3). The mechanism of GP is in very much line with GA except for the fact the solutions in GP are entire model structure whereas in GA the solutions are coefficients of the model. The following steps are listed for implementation of GP [28].

Steps:

1. The parameters of GP are set before its implementation. Parameters such as functional set consisting of airthematic operations and non-linear functions, terminal set consisting of the four inputs, population size also referred as a number of models, number of generations defined as the completion time for the iterations/evolutionary process to stop, fitness function defined as the error/objective function of the models, probabilities of genetic operations (reproduction, crossover and mutation), depth of model (size) and threshold error.

2. The initial generation/population of models is produced by combining the elements from the functional and terminal set randomly.

3. The objective/fitness function used to evaluate the error of these models against the experimental data is structural risk minimization (SRM) principle. SRM objective function also takes into account the complexity of the models along with empirical error and punishes the objective value. In this way, the local convergence is avoided.

   The objective function SRM used is as follows:

$$SRM = \frac{SSE}{N}\left(1-\sqrt{\left(\left(\frac{g}{N}-\left(\frac{g}{N}\log\left(\frac{g}{N}\right)\right)+\left(\frac{\log\left(\frac{g}{N}\right)}{2N}\right)\right)\right)}\right)^{-1} \tag{3}$$

where g is number of nodes of the model during evolutionary stages of GP, SSE is the sum of square of error of the generated model on the training data and N is the number of training samples.

4. Checking of the model performance against the stopping criterion (threshold error and maximum number of runs). If it meets the criterion, the best-fit model will be chosen according to the minimum training error. Otherwise, step 4 is implemented.

5. Ranking of models and tournament selection for the selection of models for genetic operations. Size of tournament considered in this work is 6.

6. Genetic operations such as subtree crossover, subtree mutation and reproduction with probability of 85%, 10% and 5% are applied to produce new population.

67Step 3 is again checked and if it satisfies the stopping threshold criterion, the best-fit model will be chosen according to the minimum training error. If it is not satisfied, then the subsequent steps from Step 4 are implemented.

The effective implementation of GP algorithm depends highly on the settings of the key parameters such as population size, number of generations and runs, maximum depth of the model, probabilities for genetic operations. In this work, based on sufficient number of the data samples, the population size of 300, number of generations and runs at 120 and 10 respectively, maximum depth varying from 6 to 8 and probabilities of 0.85, 0.10 and 0.05 for cross-over, mutation and reproduction respectively.

The algorithm is implemented in MATLAB R2010b and the best model for the each data set is selected based on the minimum training error. Fig. 4 shows the relation between the mean absolute percentage error (MAPE) of the best GP models for each of the 20 training data sets and its corresponding complexity (number of nodes and depth). From Fig. 4, it is clear that the lowest MAPE was achieved for the complexity measuring the number of nodes 42 and depth 8 of the GP model for data set 9. Fig. 5 shows the bar plot of MAPE of the best GP model for each on the 20 training data sets. From Fig. 5, the data set corresponding to number 9 have lowest training MAPE of 3.79 and therefore the best GP model (GP_W, Equation 4) corresponding to this data set is chosen for the analysis.

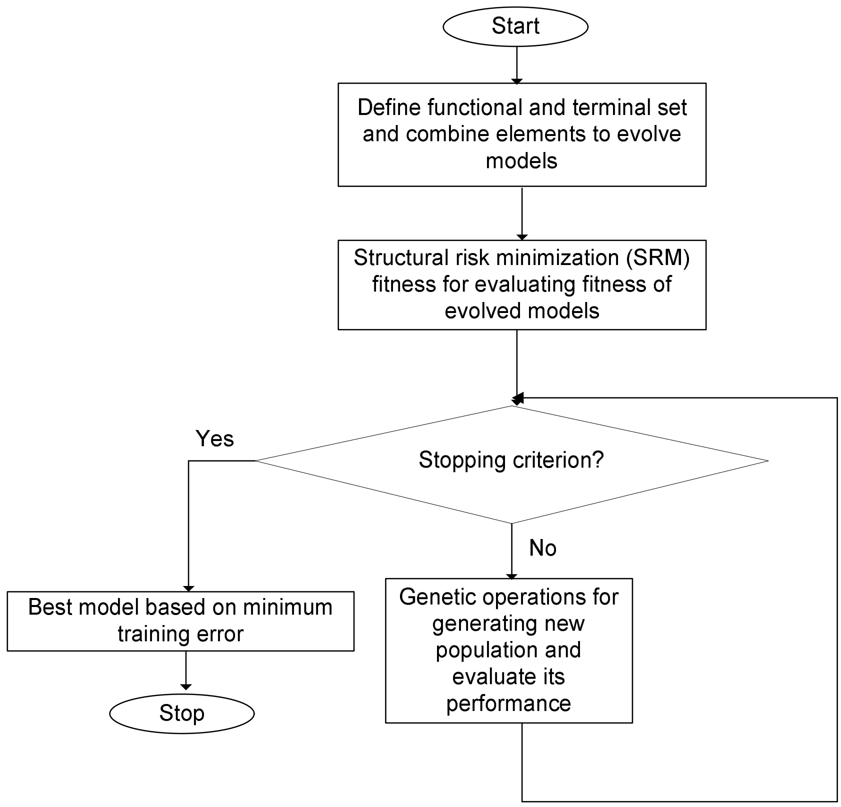

Fig. 3 Flowchart showing a stepwise process of GP

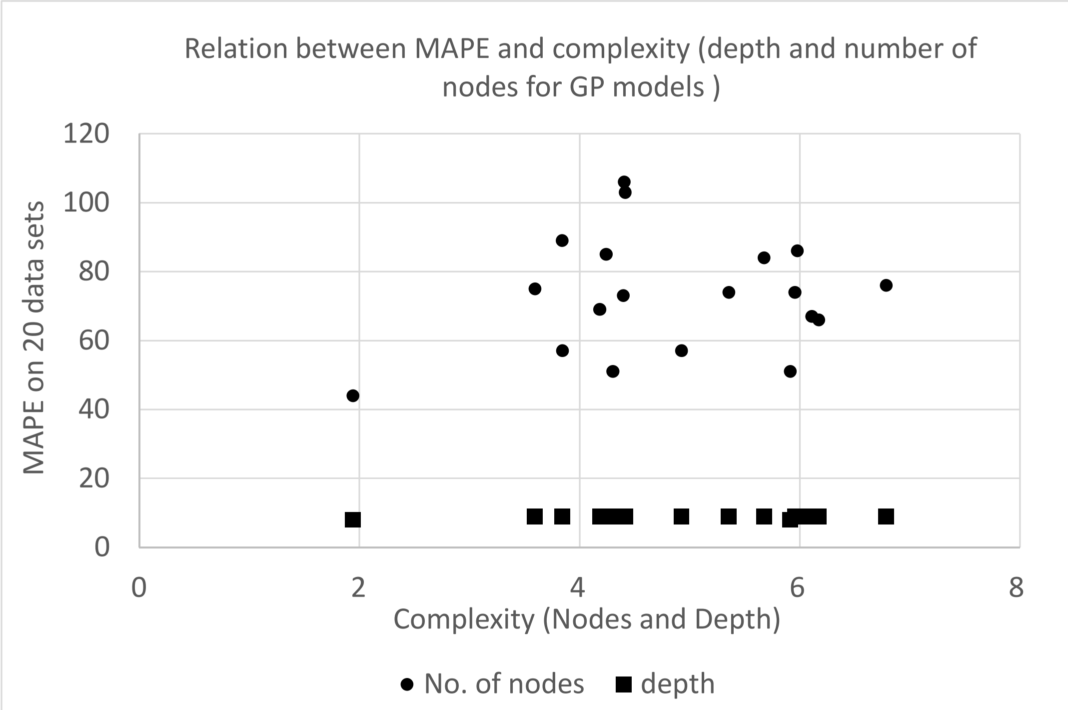

Fig. 4 Bar graph showing relation between MAPE and complexity of the GP models for each of 20 data sets

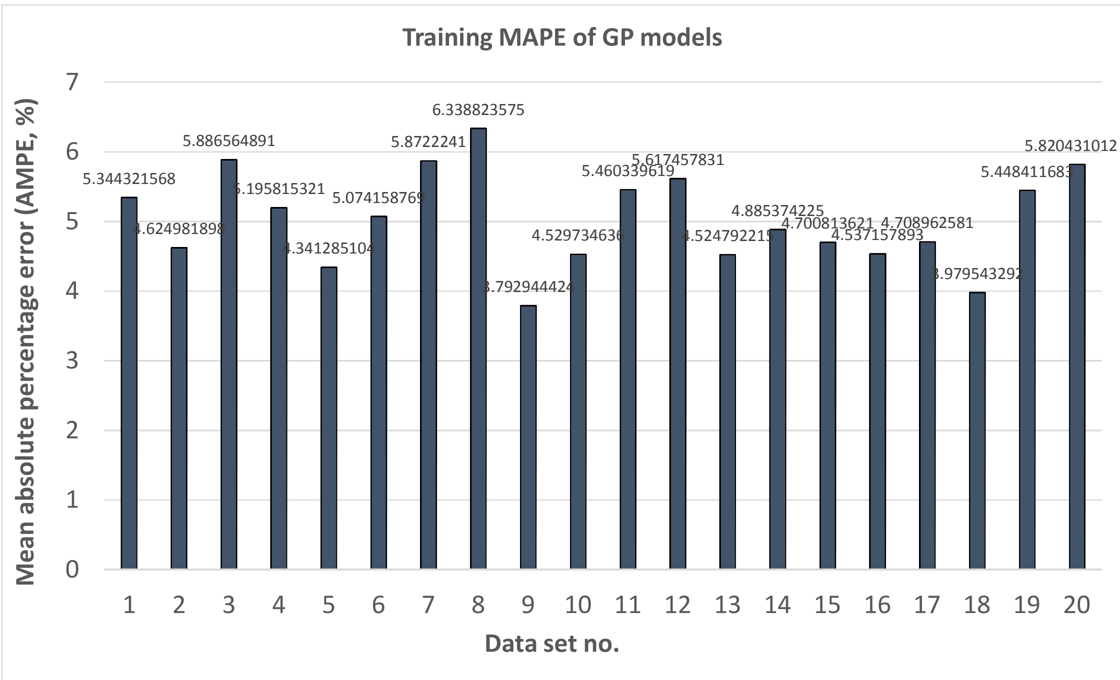

Fig. 5 Bar graph showing MAPE of GP models for each of the 20 training data sets

Wilting Point $(\%)_{GP}$ (GP_W) = -0.18771+(-0.0034925)*((sin(sin(x3)))-(x3))+(0.053496)*(sin(cos(x4)))+(0.018368)*(cos(plog(((x4)-(x2))-(cos(x2)))))+(0.0049484)*((tan((x4)-(cos(x2))))-(sin(x2)))+(-0.028685)*((plog(sin(plog((x4)-(x3)))))+(x2))+(0.0022124)*((x4)*((x4)-(cos(x3))))+(-0.00020903)*(tan((x4)-(cos((11.133678)))))+(0.057332)*(x1); (4)

where x1, x2, x3, and x4 are the Fractal dimension, S-index, clay and organic content respectively.

4. Analysis of the GP based wilting point model

In this section, the performance analysis of the GP based wilting point model (Equation 4) is evaluated against the experimental data as discussed in Section 2. The four performance measures used to evaluate the performance of GP model is given by Equations A1 to A4 in the appendix.

Table 1 clearly shows that the GP based wilting point model corresponding to data set 9 have very good training accuracy with coefficient of determination of 0.97 and lower values of MAPE of 3.79, RMSE of 0.007 and MO of 5.32. This shows that 40 training data sets were sufficient to train the GP algorithm effectively. Similarly, on the testing data the GP based wilting point model have shown higher generalization performance with coefficient of determination varying of 0.98 and lower values of MAPE, RMSE and MO. Table 2 shows the actual wilting point values, predicted wilting point values and relative error (%) of the GP model on the testing data. The curves of the predicted and actual values is shown in Figs. 6a-c. This clearly shows that the actual values of wilting point obtained experimentally is very close to those obtained from the GP based wilting point model. Fig. 7 shows the distribution of the relative error (%) of the model with respect to the entire data set. From Fig. 7a and b, a less variation of the testing error and the difference of mean of training and testing error is noticed, which indicates the good generalization ability of the model.

Further, the goodness of the fitness tests for the model is performed by *t*-test for the mean and *f*-test for the variance. *P*-values (Table 3) obtained more than 0.05 indicates that the predictions obtained from the GP based wilting point model is not significantly different from those obtained from experimental set-up.

Based on the statistical analysis conducted, it can be concluded that the GP based wilting point model is able to generalize the wilting point values satisfactorily under variation of the four inputs. The following section will discuss about the procedure for obtaining the relationships between the wilting point and the four inputs from the GP model.

Table 1 Statistical metrics of the GP based wilting point model

	R^2		RMSE (%)		MAPE (%)		Multi-objective error (MO)	
Models	**Training phase**	**Testing phase**	**Training phase**	**Testing phase**	**Training phase**	**Testing phase**	**Training phase**	**Testing phase**
Tool life (min)								
GP	0.97	0.98	0.007	0.004	3.79	1.94	5.32	1.98

Table 2. Actual, predicted and relative error of the GP based wilting point model

No.	Actual	GP_W	RE (%)
1	0.25	0.24734	1.064075
2	0.26	0.273216	5.083243
3	0.26	0.26589	2.265551
4	0.28	0.266464	4.834374
5	0.28	0.270066	3.547805
6	0.28	0.260172	7.08151
7	0.29	0.29645	2.224198
8	0.31	0.301593	2.711853
9	0.31	0.30859	0.454847
10	0.08	0.082164	2.704742
11	0.08	0.082187	2.734312
12	0.08	0.08885	11.06266

13	0.09	0.090368	0.408337
14	0.11	0.104107	5.357142
15	0.11	0.109023	0.888515
16	0.22	0.226481	2.945915
17	0.24	0.240761	0.31696
18	0.25	0.251483	0.593363
19	0.26	0.253844	2.367526
20	0.11	0.104995	4.550035

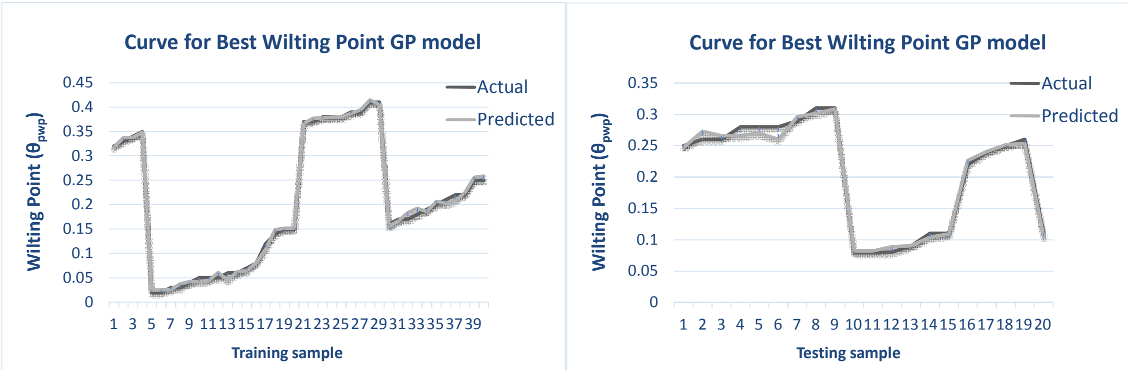

(a) **(b)**

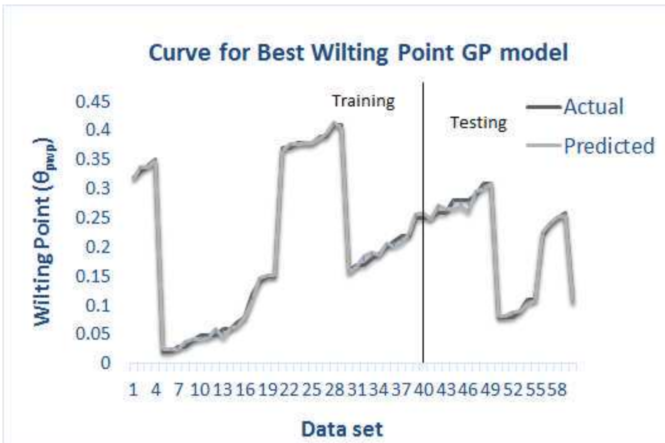

(c)

Fig. 6 Curves showing the correlation of actual and predicted values of GP based wilting point model

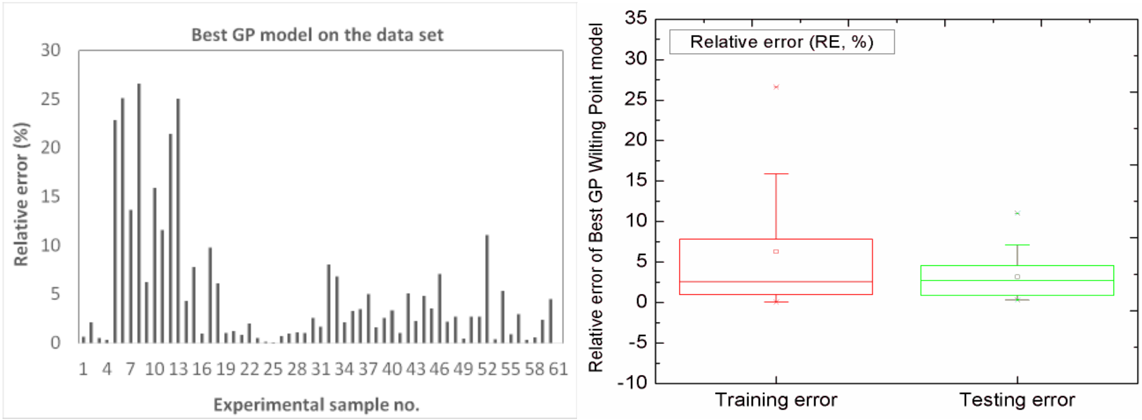

(a) (b)

Fig. 7 Distribution of relative error (%) of the GP based wilting point model across the data

Table 3. Goodness of fitness tests of the GP based wilting point model

95%CI	***p*-value**
	GP
Mean paired *t*-test	0.56
Variance *F*-test	0.90

5. 2-D and 3-D plots for main and interaction effect from the Wilting Point model

This section discusses the parametric and sensitivity analysis procedure for evaluating the main and interaction effects of the four inputs (fractal dimension, S-index, clay content and organic content) on the GP based wilting point model. The detailed mathematical procedure for the parametric and sensitivity analysis is discussed in an empirical study conducted in [20].

For measuring the main effects, each of the four inputs is vary from its minimum to maximum value. During this procedure, on varying one input, the other three inputs are kept constant at their mean level. The wilting point values are then computed from the model. The 2-D plots in Fig. 8a shows the main effects obtained for the wilting point with respect to each input, provided the other inputs are at their mean values. It clearly shows that the wilting point increases with an increase in fractal dimension and behaves highly non-linearly with respect to clay and organic content. There was hardly any change in wilting point noticed with respect to S-index. For measuring the interaction effect between the two inputs, the same procedure as for measuring the main effect is followed except that in this, the two inputs are varied at once from its minimum to maximum values. The remaining two inputs are kept fixed at their mean level. 3-D plots shown in Fig. 8b indicates that the combined effect of clay and organic content produces higher variations in wilting point followed by combined effect of pairs ((clay content and fractal dimension) and (organic content and fractal dimension)). Hardly, any variations in the wilting point were noticed for the combined effect of S-index and other inputs.

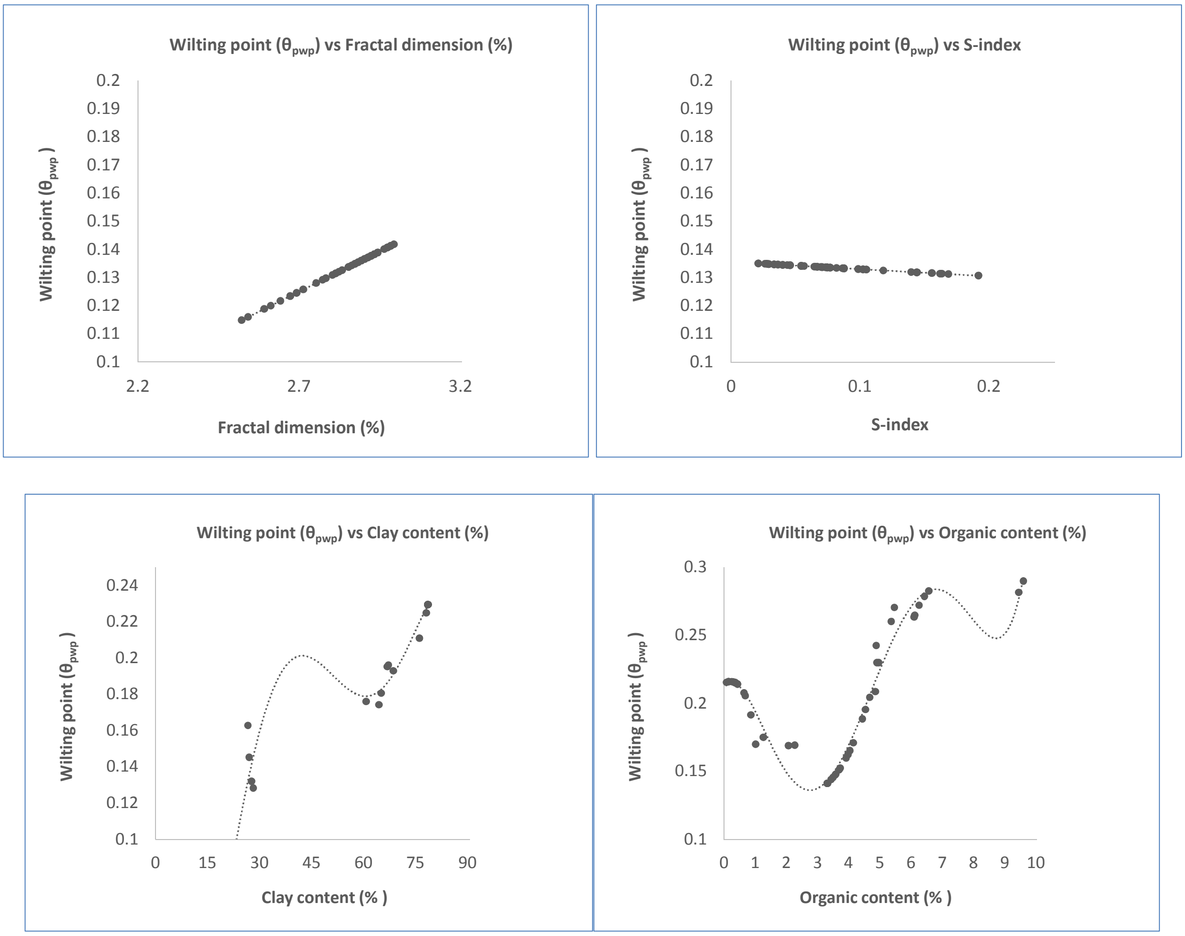

(a)

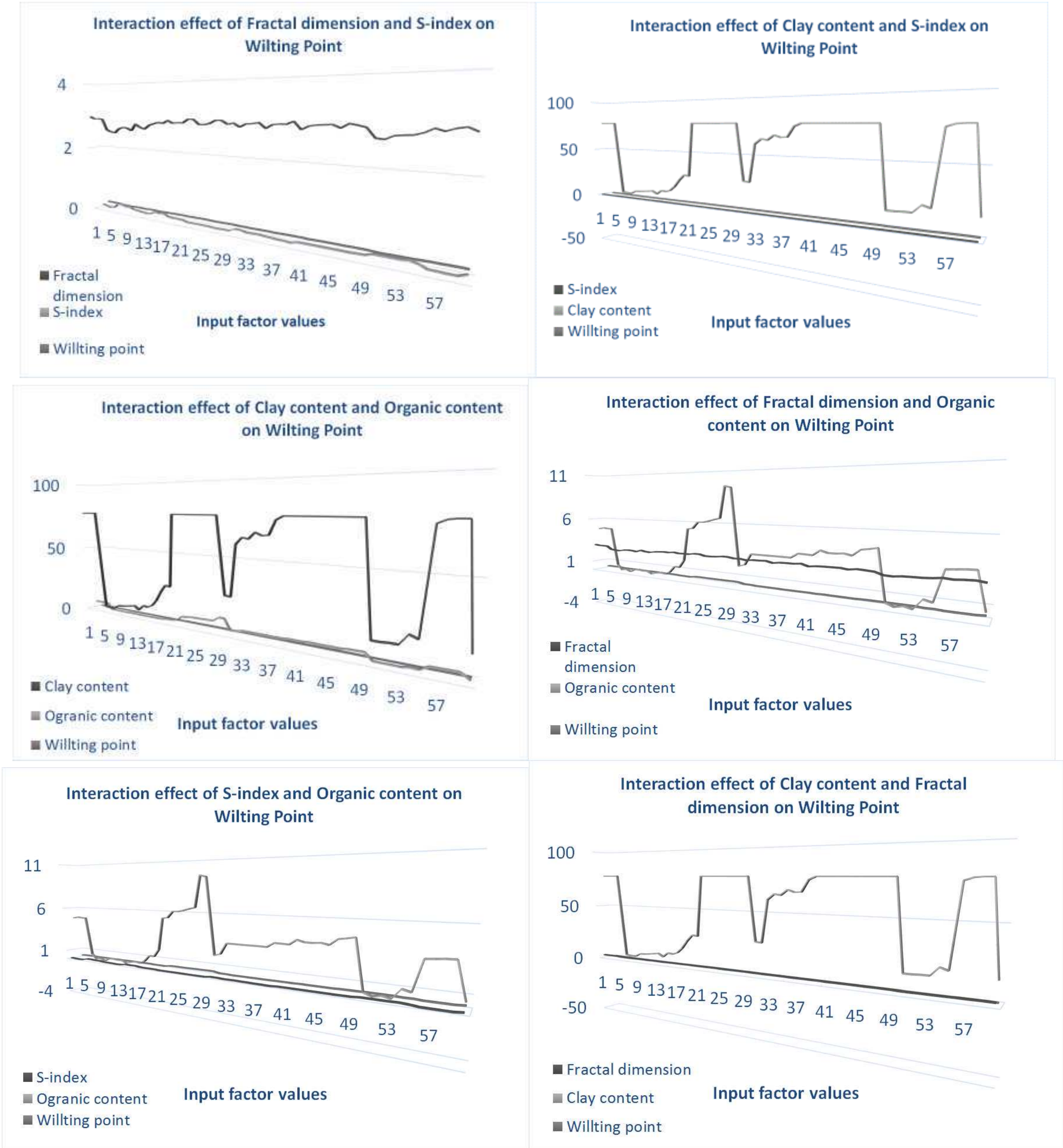

(b)

Fig. 8 2-D and 3-D plots showing the relationships of the wilting point with respect to each of the input

Further, the sensitivity analysis (Fig. 9) measuring the amount of impact of inputs on the wilting point is conducted on the wilting point model. This is done by finding the maximum and minimum from 2-D plots (Fig. 8a) and the number of peaks from 3-D plots (Fig. 8b). It is found from Fig. 9 that the clay content influence the wilting point the most followed by organic content, fractal dimension and S-index. This interpretation from the sensitivity analysis is also in line with the findings from the parametric analysis. Thus, based on this analysis an appropriate values of clay and organic content can be selected that can optimize the wilting point efficiently.

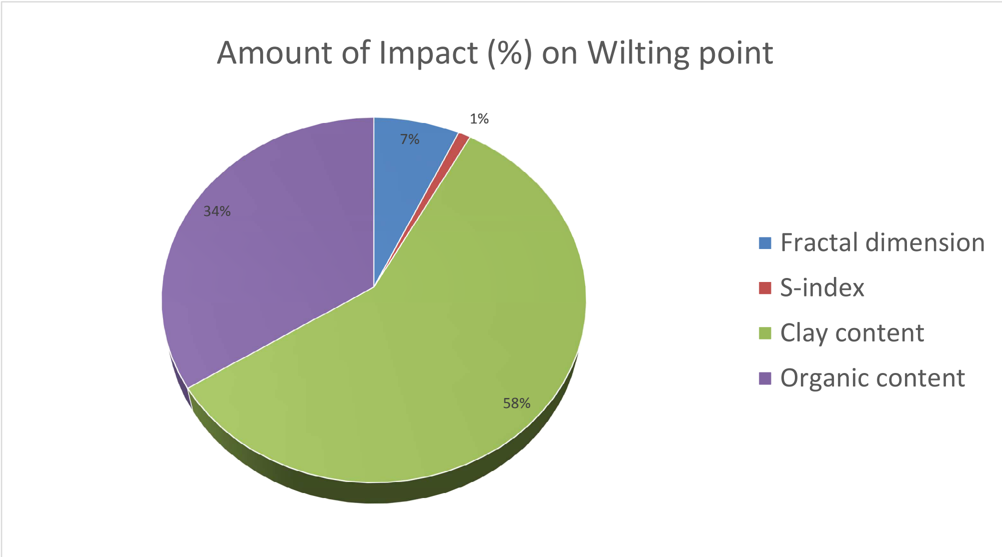

Fig. 9 Percentage contribution of input variable to wilting point

6. Conclusions

The present paper laid significant emphasis on the need of formulation of a model for evaluating the wilting point based on soil parameters. In particular in this study the following parameters have been considered: fractal dimension, S-index, clay and organic content. While many studies in literature assumed wilting point as the moisture content at a soil matric potential of -1500 kPa, the current study aims at understanding the variations in wilting point with respect to soil parameters. This objective is achieved by the design of an optimization framework of GP which resulted in formulation of generalized wilting point model with higher values of coefficient of determination and lower values of MAPE, RMSE and MO. The model obtained represents the explicit (functional) relationship between wilting point and the four soil parameter inputs and therefore can also be used for wilting point optimization. Further, the robustness of the model is evaluated by extracting the relationships between wilting point and the four inputs. The 2-D plots shows that wilting point increases with fractal dimension while behaves highly non-linear with respect to clay and organic content. 3-D plots shows that the combined effect of the clay and organic content influence the wilting point the most. The findings from this analysis is useful for experts to generalize and monitor the wilting point of soil under extreme variation of clay and organic content while giving minimum attention to fractal dimension and S-index. Future work can include sophisticated reliability analysis methods [29, 30] including dynamic neural networks [31 - 34] to monitor the wilting point in event of uncertainties in the measurements.

Acknowledgement

The authors wish to acknowledge that this research has been supported by Shantou University Scientific Research Foundation (Grant No. NTF 16002).

References

1. Steyer, R., & Peters, A. (2015). Dependency of Contact Angle on Water Content and Drying Time in the Moisture Range Below Wilting Point. Soil Science Society of America Journal, 79(2), 499-503.
2. Hosseini, F., Mosaddeghi, M. R., Hajabbasi, M. A., & Sabzalian, M. R. (2016). Role of fungal endophyte of tall fescue (Epichloë coenophiala) on water availability, wilting point and integral energy in texturally-different soils. Agricultural Water Management, 163, 197-211.
3. Da Silva, M. A., Monserrate, F., Valencia, J., Quintero, M., & Jarvis, A. (2016). Digital mapping of soil properties in the West of Honduras, Central America.
4. Nakhforoosh, A., Bodewein, T., Fiorani, F., & Bodner, G. (2016). Identification of water use strategies at early growth stages in durum wheat from shoot phenotyping and physiological measurements. Frontiers in Plant Science, 7.
5. Bonfante, A., & Bouma, J. (2015). The role of soil series in quantitative land evaluation when expressing effects of climate change and crop breeding on future land use. Geoderma, 259, 187-195.
6. Sreelash, K., Buis, S., Sekhar, M., Ruiz, L., Tomer, S. K., & Guérif, M. (2017). Estimation of available water capacity components of two-layered soils using crop model inversion: Effect of crop type and water regime. Journal of Hydrology, 546, 166-178.
7. Berretta, C., Poë, S. and Stovin, V., (2014). Moisture content behaviour in extensive green roofs during dry periods: The influence of vegetation and substrate characteristics. *Journal of Hydrology* 511: pp.374-386.
8. Poë, S., Stovin, V., and Berretta, C., (2015). Parameters influencing the regeneration of a green roof's retention capacity via evapotranspiration. *Journal of Hydrology*, 523: pp. 356-367.
9. Stovin, V., Poë, S. De-Ville, S., and Berretta, C., (2015). The influence of substrate and vegetation configuration on green roof hydrological performance. *Ecological Engineering*, 85 , pp. 159-172
10. Kirkham, M. B. (2014). Principles of soil and plant water relations. Academic Press.
11. Eden, M., Gerke, H. H., & Houot, S. (2017). Organic waste recycling in agriculture and related effects on soil water retention and plant available water: a review. Agronomy for Sustainable Development, 37(2), 11.
12. Leung, A. K., Garg, A., & Ng, C. W. W. (2015). Effects of plant roots on soil-water retention and induced suction in vegetated soil. Engineering Geology, 193, 183-197.

13. Lobet, G., Pagès, L., & Draye, X. (2014). A modeling approach to determine the importance of dynamic regulation of plant hydraulic conductivities on the water uptake dynamics in the soil-plant-atmosphere system. Ecological Modelling, 290, 65-75.
14. Dexter, A. R. (2004). Soil physical quality: part I. Theory, effects of soil texture, density, and organic matter, and effects on root growth. Geoderma, 120(3), 201-214.
15. Ghanbarian-Alavijeh, B., & Millán, H. (2009). The relationship between surface fractal dimension and soil water content at permanent wilting point. Geoderma, 151(3), 224-232.
16. Garg, A., Panda, B., & Shankhwar, K. (2016). Investigation of the joint length of weldment of environmental-friendly magnetic pulse welding process. The International Journal of Advanced Manufacturing Technology, 87(5-8), 2415-2426.
17. Panda, B. N., Bahubalendruni, M. R., & Biswal, B. B. (2014). Comparative evaluation of optimization algorithms at training of genetic programming for tensile strength prediction of FDM processed part. Procedia Materials Science, 5, 2250-2257.
18. Panda, B., Garg, A., Jian, Z., Heidarzadeh, A., & Gao, L. (2016). Characterization of the tensile properties of friction stir welded aluminum alloy joints based on axial force, traverse speed, and rotational speed. Frontiers of Mechanical Engineering, 11(3), 289-298.
19. Abhishek, K., Panda, B. N., Datta, S., & Mahapatra, S. S. (2014). Comparing predictability of genetic programming and ANFIS on drilling performance modeling for GFRP composites. Procedia Materials Science, 6, 544-550.
20. Garg, A., Panda, B. N., & Lam, J. S. L. (2016). Functional characterization of current characteristic of direct methanol fuel cell. Fuel, 183, 432-440.
21. Vardhan, H., Garg, A., Li, J., & Garg, A. (2016). Measurement of stress dependent permeability of unsaturated clay. Measurement, 91, 371-376.
22. Puckett, W. E., Dane, J. H., & Hajek, B. F. (1985). Physical and mineralogical data to determine soil hydraulic properties. Soil Science Society of America Journal, 49(4), 831-836.
23. Nemes, A., Schaap, M. G., Leij, F. J., & Wösten, J. H. M. (2001). Description of the unsaturated soil hydraulic database UNSODA version 2.0. Journal of Hydrology, 251(3), 151-162.
24. Fooladmand, H. R., & Haghighat, M. (2007). Spatial and temporal calibration of Hargreaves equation for calculating monthly ETo based on Penman‐Monteith method. Irrigation and Drainage, 56(4), 439-449.

25. Bouraoui, F., Vachaud, G., Haverkamp, R., & Normand, B. (1997). A distributed physical approach for surface-subsurface water transport modeling in agricultural watersheds. Journal of Hydrology, 203(1-4), 79-92.

26. De Gennes, P. G. (1985). Wetting: statics and dynamics. Reviews of modern physics, 57(3), 827.

27. Brooks, R. H., & Corey, A. T. (1964). Hydraulic properties of porous media and their relation to drainage design. Trans. ASAE, 7(1), 26-0028.

28. Tyler, S. W., & Wheatcraft, S. W. (1989). Application of fractal mathematics to soil water retention estimation. Soil Science Society of America Journal, 53(4), 987-996.

29. Koza, J. R. 1996. On The Programming Of Computers By Means Of Natural Selection, Mit Press, Cambridge, USA.

30. Zhang, Yi, Chul-Woo Kim, Kong Fah Tee, and Jasmine Siu Lee Lam. "Optimal sustainable life cycle maintenance strategies for port infrastructures." Journal of Cleaner Production 142 (2017): 1693-1709.

31. Robust and stepwise optimization design for CO2 pipeline transportation, International Journal of Greenhouse Gas Control, 58: 10-18, 2017.

32. A new stepwise and piecewise optimization approach for CO2 pipeline, International Journal of Greenhouse Gas Control, 49: 192-200, 2016.

33. Synchronized control with neuro-agents for leader-follower based multiple robotic manipulators, Neurocomputing, 124(26): 149-161, 2014.

34. A Framework of Neural Networks Based Consensus Control for Multiple Robotic Manipulators, Neurocomputing, 140: 8-18, 2014.

Appendix:

$$\textit{Coefficient of determination}\ (R^2) = \left(\frac{\sum_{i=1}^{n} (A_i - \overline{A_i})(M_i - \overline{M_i})}{\sqrt{\sum_{i=1}^{n} (A_i - \overline{A_i})^2 \sum_{i=1}^{n} (M_i - \overline{M_i})^2}} \right)^2 \qquad \text{(A1)}$$

$$\textit{Root mean square error}\ (RMSE) = \sqrt{\frac{\sum_{i=1}^{N} \left| M_i - A_i \right|^2}{N}} \qquad \text{(A2)}$$

$$Multiobjective\ error\ (MO) = \frac{MAPE + RMSE}{R^2} \quad \text{(A3)}$$

$$\mathrm{Re}\,lative\ error\ (\%) = \frac{\left|M_i - A_i\right|}{A_i} \times 100 \quad \text{(A4)}$$

where M_i is the value predicted by a model, and Y_i is the actual value of the output